Published In Journal Of Applied Physics J. Appl. Phys. 137, 133905 (2025)

Magneto-Optical Tuning of Ferromagnetic Resonance in Silicon-doped Yttrium Iron Garnet

Maksym A. Popov[1)], H. L. Chumak[1)], Oleksandr Klimov[1)], Yurii Shepelytskyi[2,3)], Janos Rado[4)], Alla Reznik[4)], Mitchell S. Albert[2,3,5)], Michael R. Page[6)], Gopalan Srinivasan[7, *)]

[1)] Educational and Scientific Institute of High Technologies, Taras Shevchenko National University of Kyiv, Kyiv 01601, Ukraine

[2)] Department of Chemistry, Lakehead University, Thunder Bay, Ontario P7B 5E1, Canada

[3)] Thunder Bay Regional Health Research Institute, Thunder Bay, Ontario P7B 6V4, Canada

[4)] Department of Physics, Lakehead University, Thunder Bay, Ontario P7B 5E1, Canada

[5)] Northern Ontario School of Medicine, Thunder Bay, Ontario P7B 5E1, Canada

[6)] Materials and Manufacturing Directorate, Air Force Research Laboratory, Wright-Patterson Air Force Base, Dayton, Ohio 45433, USA

[7)] Department of Physics, Oakland University, Rochester, MI 48309, USA

Abstract

This report is on experiments and theory on the process of optically stimulated electron population density redistribution in Si-substituted yttrium-iron garnet single crystals at 77 K. It was determined that a photo-induced uniaxial anisotropy field arose in YIG:Si sample in response to illumination by quasi-linearly polarized laser (λ=808 nm) laser leading to redistribution of Fe^{2+} ions among the nonequivalent octahedral sites. The photo-induced field was measured by

variation of ferromagnetic resonance (FMR) frequency in the X-band. The measured FMR frequency shift demonstrated a pronounced dependence on the polarization vector orientation with respect to crystallographic axes, in accordance with the theory discussed here. The frequency shift dependence on light intensity (for optimal polarization orientation) was found to be nearly linear, at least within the output intensity range of the optical source. The maximum frequency shift was –130 MHz for 75 mW applied optical power. A similar phenomenon was also observed at room temperature, but was attributed to the sample heating by the incident light. The results presented here demonstrate the potential of the phenomenon for application in the development of ferrite signal processing devices with dual tuning by both magnetic field and optical irradiation.

- Corresponding author: srinivas@oakland.edu

1. Introduction

It is known that in silicon-doped iron-yttrium garnet (YIG) single-crystals it is possible to vary the magnetic parameters and magnetic ordering by thermomagnetic or photomagnetic effects [1-2]. The underlying phenomena responsible for such variations include photoinduced spin-reorientation transitions [3], polarization reconstruction of the domain structure of garnet film [4], changes in ferromagnetic resonance (FMR) frequency [5,6], magnetic anisotropy [7,8], domain wall resonance [1], and spin-wave resonance spectra of Si:YIG thin films [9]. The influence of thermo- or photo treatment on the properties of $Y_3Fe_{5-x}Si_xO_{12}$ (denoted as Si:YIG) can be attributed to thermo- or photoactivated hopping of weakly coupled electron between iron ions in the octahedral sites. The ferrous, Fe^{2+}, ions are present in the crystal lattice as a result of the partial substitution of $Si^{4+}$for trivalent iron in stoichiometric YIG. The presence of both divalent and trivalent leads to hopping of electrons between the iron ions. Such hopping will result in increased conductivity of the doped specimens in comparison to the Si-free samples and will also modify the magnetic anisotropy since divalent Fe ions are strongly anisotropic and their contribution to net anisotropy energy per ion is large [10, 11].

In the crystal lattice of garnets, the Fe^{2+} ions preferably occupy octahedral crystallographic sites [2]. Four kinds of such octahedral sites exist in a unit cell of YIG with each site having its own trigonal crystal field with a local symmetry axis coinciding with one of the four body-diagonal directions of the cubic unit cell. The effects associated with Fe^{2+} result from the migration of the electrons between ferrous ions in the aforementioned four different positions [5] under the influence of various external (electric field, magnetic field light illumination) or internal (temperature) stimuli. Specifically, this report focuses on investigation of electron hopping process caused by absorption of photons from external source. The energy acquired in the process allows the electron from divalent Fe^{2+} to leave the local potential well and move to some other trivalent Fe^{3+} atom. Then the iron atom at the former location of the electron will turn from Fe^{2+} to Fe^{3+} and iron in current location from Fe^{3+} to Fe^{2+}. Whereas Fe atoms physically remain in their places during this process, the hopping of extra electrons between octahedral sites

leads to effective changes in Fe^{2+} populations in those sites (the total number of ferrous ions remains the same, being determined by the amount of Si doping, only their distribution varies). In the absence of an external magnetic field and at a rather high temperature (for which valence exchange is possible i.e. the electron kinetic energy is greater than the potential barrier between sites), all the sites are populated with equal probability and their total contribution to the magnetic anisotropy will compensate each other. However, at low temperatures, when the thermal energy is lower than the potential barrier, the hopping of electrons is mainly determined by the energy absorption from the incoming photons, which in turn, depends on light polarization orientation. Thus, by carefully choosing the incident light electric field vector direction with respect to the crystal axes it is possible to make one of the sites a preferred one (i.e., increase the occupancy of one type of sites at the expense of the other three). Such population imbalance between different sites can produce an induced uniaxial magnetic anisotropy constant and an associated effective anisotropy field [2, 4].

For example, it is known that under the application of an external magnetic field, the Fe^{2+} will preferably occupy a site whose local axis makes a smaller angle with the magnetization direction $\vec{M}$ than divalent Fe in other sites [6]. Consequently, a change of magnetization direction with respect to crystallographic axes will result in the modification of Fe^{2+}-induced anisotropy. This phenomenon is known as photo-magnetic annealing [5]. Alternately, for a fixed orientation of $\vec{M}$, the quasi-equilibrium distribution of ion populations may be perturbed by the illumination of a sample with optical or near infrared radiation. As explained above, the absorbed photons will strip the “extra” electrons from divalent iron ions, and those electrons will hop to trivalent iron ions at other sites and converting them to Fe^{2+}. Such photo-stimulated electron transitions between different sites change the magneto-crystalline anisotropy, which in turn affects the domain structure, magnetic permeability, spin-wave dispersion, etc [2, 12]. The above mentioned effects, which indeed depend on both on the light intensity and polarization, were previously reported in Si:YIG [1, 4 ,7]. Regarding magneto-crystalline anisotropy, there are several past reports on experimental evidences with the use of near-infrared irradiation. The

anisotropy of silicon-doped yttrium iron garnet could be changed by 21 Oe at 66 K, by more than 100 Oe at 20 K [5]; by 20 Oe at 77 K [8], and by 60 Oe at 4.2 K [13] through such irradiation. Most of these experiments were done at cryogenic temperatures since the low thermal energy of electrons prevents them from hopping back to their original sites and restoring equilibrium distribution (at least during the duration of measurements) thus making phenomena observable.

This work is devoted to investigation of the effects of light irradiation on the magnetostatic mode frequencies in a disk-shaped sample of single crystal Si:YIG with the chemical composition $Y_3Fe_{4.49}Si_{0.51}O_{12}$ at room temperature (300 K) and at liquid nitrogen (77 K) temperature. The mode frequencies depend on the magneto-crystalline anisotropy field. Since the change in the anisotropy field is shown to be influenced by optical radiation in this work, this phenomenon provides a new path to effectively tune the magnetic resonance frequencies by exposing the magnetic crystal to light. This may be a viable alternative to the conventional way of frequency tuning by changing the external magnetic field with an electromagnet or a solenoid and makes possible miniaturization of magnetic devices and reduce their weight and power requirements.

2. Theory

a) Photoinduced variations in octahedral site Fe^{2+} population

We will utilize the model previously developed in [12] for the theoretical explanation of the observed magnetooptical phenomenon. According to this model, the probability of a given electron's transition from some octahedral site labeled i (i=1,2,3,4) to any of the three other non-equivalent sites comprises a sum of photoinduced and thermoactivated transition probabilities and is given by

$$W_i = KI(1 + B\cos^2(\Psi_i)) + \nu e^{-\frac{Eact}{kT}} \quad (1)$$

Here K and B are some phenomenological constants, I is the optical radiation intensity and Ψ_i is the angle between the octahedral site's local trigonal symmetry axis and the electric field vector of the optical radiation (i.e. polarization vector $\vec{P}$). Local symmetry axes are directed along one of the four possible $[\pm1\pm1\pm1]$ directions. Since K and B are assumed the same for all sites, the difference in probability of optically stimulated electronic transition from a given site is determined only by the relative orientation of vector $\vec{P}$ and local trigonal axis given by Ψ_i. The second term in (1) is the probability of thermally activated hops, where E_{act} is the activation energy of transitions, and ν is the frequency factor.

Upon cooling a specimen to a cryogenic temperature, the thermoactivated electron diffusion becomes less important and photoinduced effects may manifest itself to the full extent. The temporal kinetics of electrons distribution between octahedral sites is then described by the following set of equations:

$$\begin{aligned} &\frac{dn_i}{dt} = -3W_i n_i + \sum_{j=1, j\neq i}^{4} W_j n_j, \\ &\sum_{i=1}^{4} n_i = 1 \end{aligned} \tag{2}$$

where n_i , i=1,2,3,4, is the relative population density of active Fe^{2+} atoms in i-type site and W_i is given by (1). We then further specify that the polarization vector lies in (110) crystallographic plane and, correspondently, the light propagation vector (wave vector) is oriented along [110] direction. Under these conditions, two of the trigonal axes, namely [-111] and [-11-1] lay in the sample plane, whereas two others ([111] and [11-1]) are oblique to this plane. The two latter octahedral sites always have equal transition probabilities W_i, regardless of $\vec{P}$ orientation, and thus their populations also will be equal.

If the sample is exposed to photons for a time long enough to achieve an equilibrium distribution, the site populations become [2, 12]

$$\begin{aligned} &n_{[111]} = n_{[11-1]} = \frac{W_{[-111]}W_{[1-11]}}{W}, n_{[-111]} = \frac{W_{[111]}W_{[1-11]}}{W}, n_{[1-11]} = \frac{W_{[111]}W_{[-111]}}{W}, \\ &W = 2W_{[-111]}W_{[1-11]} + W_{[111]}(W_{[-111]} + W_{[1-11]}) \end{aligned} \tag{3}$$

where the subscripts explicitly indicate the site's local symmetry axis orientation. The anisotropic energy density associated with all those Fe^{2+} atoms is given by [12]

$$E_a = N\sum_{i=1}^{4} n_i E_i,\ \ E_i = -2\lambda\cos^2\xi_i \tag{4}$$

Where λ is the constant of spin-orbital coupling, N is the total population density of ferrous atoms and ξ_i is the angle between the magnetization vector $\vec{M}$ and the direction of the local trigonal axis at i-type site. Note that the actual population density N of Fe^{2+} ions may be much lower than the concentrations of silicon dopant atoms [14]. One possible reason is that some of the imbalance Si^{4+} charge might be compensated by other bivalent impurities (e.g. Pb^{2+}) that enter the crystal lattice during crystal growth [2, 15].

The equation for anisotropic energy may be rewritten in terms of α_i – the directional cosines of magnetization vector with respect to [100], [010], and [001] axes of the cubic coordinate system, resulting in

$$E_a = -\frac{4}{3}\lambda N\left(\alpha_1\alpha_2(4n_{[111]}-1)+\alpha_1\alpha_3(n_{[1\text{–}11]}-n_{[\text{–}111]})-\alpha_2\alpha_3(n_{[1\text{–}11]}-n_{[\text{–}111]})\right) \tag{5}$$

This formula represents a completely valid expression for the magnetic anisotropy energy density; however, it is not very suitable for the description of the photomagnetic influence on the FMR frequency. To make it more convenient, we apply to Eq.(5) a standard procedure of quadratic form diagonalization [16]. After some calculations, we obtain the following set of eigenvalues and eigenvectors of the given problem:

$$\lambda_1 = \frac{x}{2}, \lambda_2 = \frac{-x+\sqrt{x^2+8y^2}}{4}, \lambda_3 = \frac{-x-\sqrt{x^2+8y^2}}{4}$$

$$\vec{V}_1 = \begin{pmatrix}1\\1\\0\end{pmatrix}, \vec{V}_2 = \begin{pmatrix}1\\-1\\y/\lambda_2\end{pmatrix}, \vec{V}_3 = \begin{pmatrix}1\\-1\\y/\lambda_3\end{pmatrix} = \begin{pmatrix}1\\-1\\-2\lambda_2/y\end{pmatrix} \tag{6}$$

here we used the following notation $x = 4n_{[111]} - 1, y = n_{[1\text{–}11]} - n_{[\text{–}111]}$. The three eigenvectors (6) are mutually orthogonal with $\vec{V}_1$ having a fixed direction whereas $\vec{V}_2$ and $\vec{V}_3$ orientation depend on specific values of population densities n_i (though always remain in the (110) plane).

In order to clarify the situation the subsequent numerical calculations were undertaken. The polar angles δ_2, δ_3 between vectors $\vec{V}_2$, $\vec{V}_3$ and [001] axis were calculated, using the magnetic material parameters given in [12]. It was found, that with the exception of rather narrow polarization orientation angle range of ≈10°, the $\delta_{2,3}$ (φ) dependencies are rather smooth and thus may be properly approximated with their average value (Fig.S5-Supplement).

Thus, below the above-mentioned restricted angle's range, the calculated average values are $<\delta_2>\approx-55°$ and $<\delta_3>\approx34°$ which corresponds to eigenvectors

$$\vec{V}_2 = \begin{pmatrix} 1 \\ -1 \\ -0.97 \end{pmatrix}, \vec{V}_3 = \begin{pmatrix} 1 \\ -1 \\ 2.06 \end{pmatrix} \tag{7}$$

Similarly, above the discarded angles, the average values are $<\delta_2>\approx54°$ and $<\delta_3>\approx-36°$ with

$$\vec{V}_2 = \begin{pmatrix} 1 \\ -1 \\ 1.01 \end{pmatrix}, \vec{V}_3 = \begin{pmatrix} 1 \\ -1 \\ -1.97 \end{pmatrix}. \tag{8}$$

Judging from the obtained results it is tempting to assume that (with some measure of error) the eigenvectors for the quadratic expression for the anisotropy energy coincides with cubic ferrite <111> and <112> cardinal directions in a whole range of polarization orientation angle φ.

As far as that assumption remains correct, we have from (6) that $y/\lambda_2 = \mp 1$ and $y/\lambda_3 = \pm 2$. Those equations, in turn, are satisfied when $y = \pm x$ and $x < 0$. Then we get the final expression for eigenvalues

$$\lambda_1 = \frac{x}{2}, \lambda_2 = -x, \lambda_3 = \frac{x}{2} \tag{9}$$

and approximate formula for the anisotropy energy is:

$$E_a = -\frac{4}{3}\lambda N\left(\frac{x}{2}\beta_1^2 - x\beta_2^2 + \frac{x}{2}\beta_3^2\right) \tag{10}$$

Here β_i are the directional cosines of magnetization vector $\vec{M}$ with respect to <110>, <1-11> and <1-12> crystallographic directions. Making use of the equation $\beta_1^2 + \beta_2^2 + \beta_3^2 = 1$ we obtain, finally

$$E_a = const + 2\lambda N x \beta_3^2 = const + 2\lambda N (4n_{[111]} - 1)\beta_2^2 \qquad (11)$$

Expression (11) shows that due to the imbalance between population densities at different octahedral sites the ferrite acquires an effective uniaxial anisotropy with an anisotropy axis oriented along <111> direction (in cubic crystal coordinates) and anisotropy constant $K_u = 2\lambda N(4n_{[111]} - 1)$. Since site population $n_{[111]}$ depends on both the intensity and polarization orientation of the incoming light beam, the anisotropy constant will depend on those quantities too, thus justifying a theoretical background for the experimentally observed photomagnetic effect.

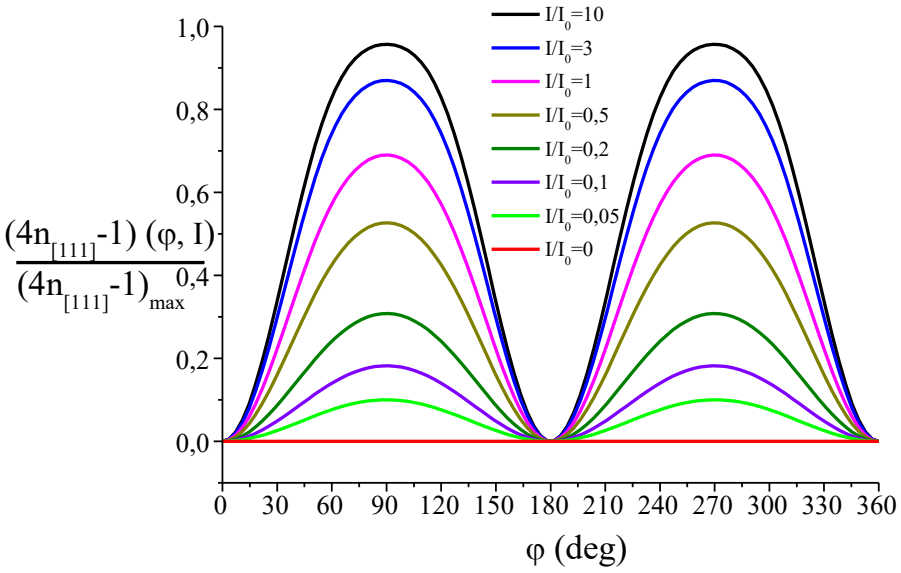

Fig. 1. *Normalized* $(4n_{[111]} - 1)$ *term dependence on polarization orientation angle φ for different values of normalized optical power I/I₀=0, 0.05, 0.1, 0.2, 0.5, 1, 3, 10.*

Figure 1 shows the calculations of the $(4n_{[111]} - 1)$ term that defines the uniaxial anisotropy constant as a function of polarization orientation angle φ with respect to <001> axis for different values of incident optical power, using expressions (1) and (3). In those formulas, Ψ_i is straightforwardly expressed via φ; parameters B, E_{act}, and ν are taken from Ref. [12], and the optical power is normalized by replacing $I \rightarrow I/I_0$, where $I_0 = 1/K$. We can see that for all values of normalized power the photoinduced anisotropy, demonstrate qualitatively similar behavior: two

local maxima and two local minima are seen with their angle position being independent of I/I_0. When I/I_0=0 there is no preferential site for hopping electrons (all W_i are equal) and uniaxial anisotropy is absent for all possible angles φ, as expected. If optical power increases, the corresponding curve also increases its spread, however for I/I_0>>1 the maximum value reaches saturation. This is also expected, since then the optically stimulated electronic transition probabilities become much larger than probabilities of thermally activated hopping (Eq.1) resulting in all W_i being essentially proportional to intensity I. Yet in this case intensity prefactors in nominators and denominators of Eq.(3) cancel each other and population densities n_i values become intensity-independent. Hence, for the sake of clarity, instead of $(4n_{[111]}-1)\,(\varphi, I)$, the data on Fig. 1 shows the renormalized value $(4n_{[111]}-1)\,(\varphi, I)/(4n_{[111]}-1)_{\max}$, where $(4n_{[111]}-1)_{\max} = (4n_{[111]}-1)(\varphi, I\to\infty)$ is the maximum possible value of this term, corresponding to the case $I\to\infty$.

Numerical calculations showed that maxima take place exactly at φ=90° and 270° and minima - at φ=0°, 180°. The next figure shows the dependence of this maximum value, calculated at φ=90°, on normalized optical power. It is seen that for low values of I/I_0, this dependence is close to linear, however for large values I/I_0>5 it tends to saturation as discussed before. Notice also, that the light intensity effect on induced anisotropy is much stronger for low power levels than for large. In other words, the same variation of laser intensity I with respect to a small starting value results in a much larger variation of induced anisotropy than for a large starting value. That may be important e. g. if this effect is to be used for microwave frequency modulation.

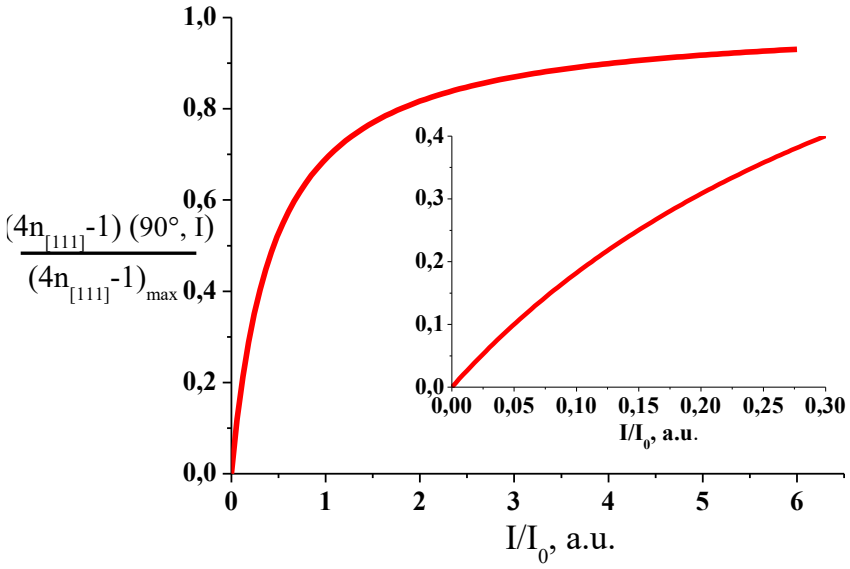

Fig. 2. *Normalized maximum value of* $(4n_{[111]}-1)$ *term vs. normalized optical power* I/I_0. *Inset shows the same curve for low values of I in the enhanced scale.*

The data on the phenomenological constant K is scarce in the literature. By combining data given in [12] and in [17], we were able to estimate K as being approximately 0.06 $cm^2/(W \cdot s)$. Then evaluating the maximum laser intensity for our specific experimental configuration (see section on Experimental setup) as $I^{max} = \frac{P_{opt}^{max}}{\pi D^2 / 4}$ where P_{opt}^{max} =75 mW, D=0.25 cm, we calculate the maximum normalized intensity as $I^{max}/I_0 \approx 0.09$. Thus the available during the experiments optical power corresponds to the initial part of the $(4n_{[111]}-1)$ vs. I/I_0 curve, shown in Fig. 2 (see inset for more a detailed view).

b) Ferromagnetic resonance frequency and photoinduced uniaxial anisotropy

The presence of additional uniaxial anisotropy due to the photomagnetic effect will manifest itself (among others) in the photoinduced changes of FMR frequency, given the other experimental conditions (bias field, temperature, etc) remain the same.

The proper account of the uniaxial anisotropy effect on the FMR was fulfilled by solving the Landau-Lifshitz equation of motion of magnetic moments with additional effective magnetic

field term $\vec{H}_{eff} = -\frac{\partial E_a}{\partial \vec{M}}$ arising from anisotropy energy [18]. The details of calculations are given in [18] and the final expression is:

$$f = \gamma \sqrt{H_0 \cos(\theta_H - \theta) + 4\pi M (N_y - N_z) + H_u \cos(2\theta)} \times \sqrt{H_0 \cos(\theta_H - \theta) + 4\pi M (N_x - N_z) + H_u \cos^2(\theta)} \quad (12)$$

Here θ is the angle between the static magnetization vector $\vec{M}$ and uniaxial anisotropy axis, θ_H – same for the bias magnetic field $\vec{H}_0$, N_z – demagnetizing factor in the direction of the bias field, N_x, N_y - demagnetizing factors in two other cardinal directions. Angles θ and θ_H are related by the additional static equilibrium condition $\sin(\theta_H - \theta) = \frac{H_u}{H_0}\sin(\theta)\cos(\theta)$. Here

$$H_u = \frac{2K_u}{M_0} = \frac{4\lambda N}{M_0}(4n_{[111]} - 1) \quad (13)$$

the photoinduced uniaxial anisotropy field magnitude.

Let's apply Eq. (12) to the situation when the sample has a shape of disk, $\vec{H}_0$ is in the sample's plane and directed along [001] crystallographic axis. Assuming $H_0 >> H_u$ we obtain $\theta=\theta_H$, thus $\vec{M}$ is also directed along [001]. The angle between $\vec{M}$ and [1-11] (anisotropy axis direction, see previous subsection) is then equal to $\theta=\arccos\left(\sqrt{\frac{1}{3}}\right)$. Since the magnetic field lies in the sample's plane, we set $N_z = N_\parallel$, correspondently, $N_y = N_\parallel$, $N_x = N_\perp$.The effect of naturally present cubic anisotropy field is taken into consideration by substitution $H_0 \to H_0 + 2H_k$, see [18]. By making all these substitutions we obtain

$$f = \gamma \sqrt{(H_0 + 2H_k - \frac{1}{3}H_u)(H_0 + 2H_k + 4\pi M (N_\perp - N_\parallel) + \frac{1}{3}H_u)} \quad (14)$$

Finally, by expanding Eq.(14) in series of ascending powers of H_u and neglecting quadratic and other terms we get

$$f \approx \gamma\sqrt{(H_0+2H_k)(H_0+2H_k+4\pi M(N_\perp-N_\parallel))}+$$
$$+\gamma\frac{H_u}{6}\left(\frac{\sqrt{H_0+2H_k}}{\sqrt{H_0+2H_k+4\pi M(N_\perp-N_\parallel)}}-\frac{\sqrt{H_0+2H_k+4\pi M(N_\perp-N_\parallel)}}{\sqrt{H_0+2H_k}}\right) \quad (15)$$

Equation (15) shows that for small values of H_u the anisotropy induced FMR frequency variation is linearly proportional to the H_u value:

$$\Delta f_r(P_{opt}) = f_r(P_{opt}) - f_r(P_{opt}=0) =$$
$$=\gamma\frac{H_u(P_{opt})}{6}\left(\frac{\sqrt{H_0+2H_k}}{\sqrt{H_0+2H_k+4\pi M(N_\perp-N_\parallel)}}-\frac{\sqrt{H_0+2H_k+4\pi M(N_\perp-N_\parallel)}}{\sqrt{H_0+2H_k}}\right) \quad (16)$$

In turn, $H_u(P_{opt})$ magnitude is defined by $(4n_{[111]}-1)$ coefficient that was analyzed in detail in the previous subsection.

3. Experimental Setup and Sample Characterization

The ferrimagnetic oxide investigated in this work was a disk-shaped sample of single crystal Si:YIG with the chemical composition $Y_3Fe_{4.49}Si_{0.51}O_{12}$. It was cut in such way that the surface normal corresponds to <110> crystallographic direction. Thus, the sample's top and bottom surfaces corresponded to (110) plane. The sample diameter and thickness were D=2.5 mm, h=0.27 mm respectively.

a. Structural characterization

The sample was characterized by Raman and X-ray diffraction (XRD) spectroscopies to study the crystal structure. The sample surface was evaluated under optical microscope. The surface was quite inhomogeneous with multiple "hills" and "valleys" (Fig. 3A). The Raman spectra were acquired using a Raman spectrometer (Renishaw, Wotten-under-Edge, UK) with a resolution of 1 cm^{-1}. The spectra were acquired with a 532 nm laser line and 1200 lines/mm grating. The system was originally calibrated with a silicon peak at 520 cm^{-1} prior to the measurements. The obtained spectra from the uneven surfaces matched each other (Fig. 3B), albeit the intensity of the Raman peaks acquired from the "valley" was significantly higher.

Thirteen peaks were observed in the spectra, two of which corresponded to the A_{1g} mode (502.45 cm^{-1} and 732.72 cm^{-1}), four corresponded to the E_g mode (268.88 cm^{-1}, 415.59 cm^{-1}, 450.44 cm^{-1}, and 588.44 cm^{-1}), and the rest corresponded to the T_{2g} modes (128.69 cm^{-1}, 170.69 cm^{-1}, 191.61 cm^{-1}, 236.27 cm^{-1}, 342.54 cm^{-1}, 374.76 cm^{-1}, and 687.7 cm^{-1}). The spectra correlated well with a known Raman spectrum of YIG [19-21] indicating the garnet structure of the sample. The magnitude and the sharpness of Raman peaks are indicative of monocrystalline sample.

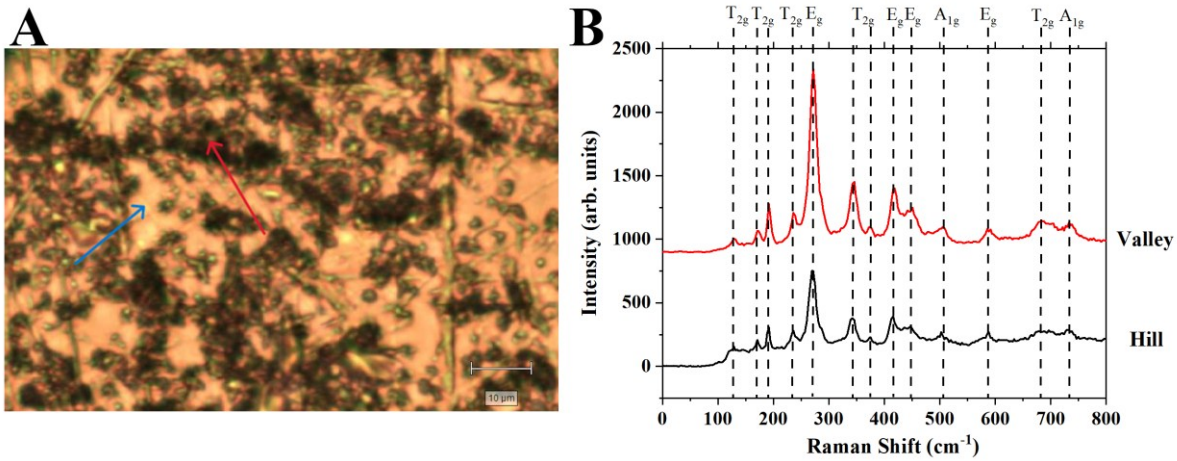

Fig 3. *A) A micrograph of the Si:YIG sample surface acquired using optical microscopy. The blue arrow indicates "valley", whereas the red arrow pinpoints "hill". B) Raman spectra acquired from the "hill" and the "valley" on the Si:YIG surface. Both spectra correlate well with each other, albeit the Raman peaks obtained from the "valley" had significantly higher intensity.*

The XRD was performed using a diffraction angle range of 20-90° with Fe Kα radiation (λ = 1.93735 Å). The XRD spectrum confirmed monocrystalline nature of the studied sample (see Supplementary Materials Fig. S1). The lattice constant was calculated from d-spacing using the equation:

$$a = d_{hkl}\sqrt{h^2 + k^2 + l^2}, \tag{17}$$

where (hkl) are Miller indices [22]. The lattice constant calculated from the XRD spectrum was equal to 12.336 Å, which is in a perfect agreement with lattice parameters in YIG doped with Si reported by Torres C., et. al. [23].

The chemical composition of the Si:YIG sample was identified using X-ray photoelectron spectroscopy (XPS). The experiments were conducted using a Kratos AXIS Supra XPS spectrometer (Kratos Analytical Ltd., Manchester, UK). In order to access potential variations of chemical composition between the sample surface and volume, a series of 6 consecutive surface etchings with focused energetic Ar ion beam after initial surface XPS spectrum acquisition was conducted. The XPS spectrum was acquired after each etching. The obtained XPS peaks of Fe 2p, Si 2p, Y 3d, and O 1s are shown in Fig. 4 A-D, respectively. The obtained surface spectrum (insets in Fig. 4 A-D) had the lowest intensity. The chemical composition of the surface was calculated to be $Y_3Fe_{4.44}Si_{0.56}O_{12}$. In addition, the spectra acquired from the surface and after the first ion etching indicated a strong presence of SiO_2 (Si 2p peak at 102.7 eV and O 1s peak at 532.5 eV). The subsequent etching of the Si:YIG sample resulted in further increase in the intensity of the Si peak at 94.3 eV and O peak at 530.7 eV. The O peak became similar to the peak conventionally observed from YIG samples [24], albeit a small shoulder at 532.5 eV was still present. The Si spectra had peaks at 100.2 eV and 102.7 eV, although the intensity of the latter became smaller. There were no significant differences between Si:YIG XPS spectra acquired after the third and all subsequent etchings. The Y spectra were not affected by the etching. The composition the interior of the Si:YIG sample was confirmed to be $Y_3Fe_{4.49}Si_{0.51}O_{12}$. Utilizing the obtained sample compositions, the density of the Si:YIG was calculated from the XRD spectrum using a procedure similar to the one in Ref.[25] and was equal to 5.122 g/cm^3, which is slightly smaller than the density of the pure YIG.

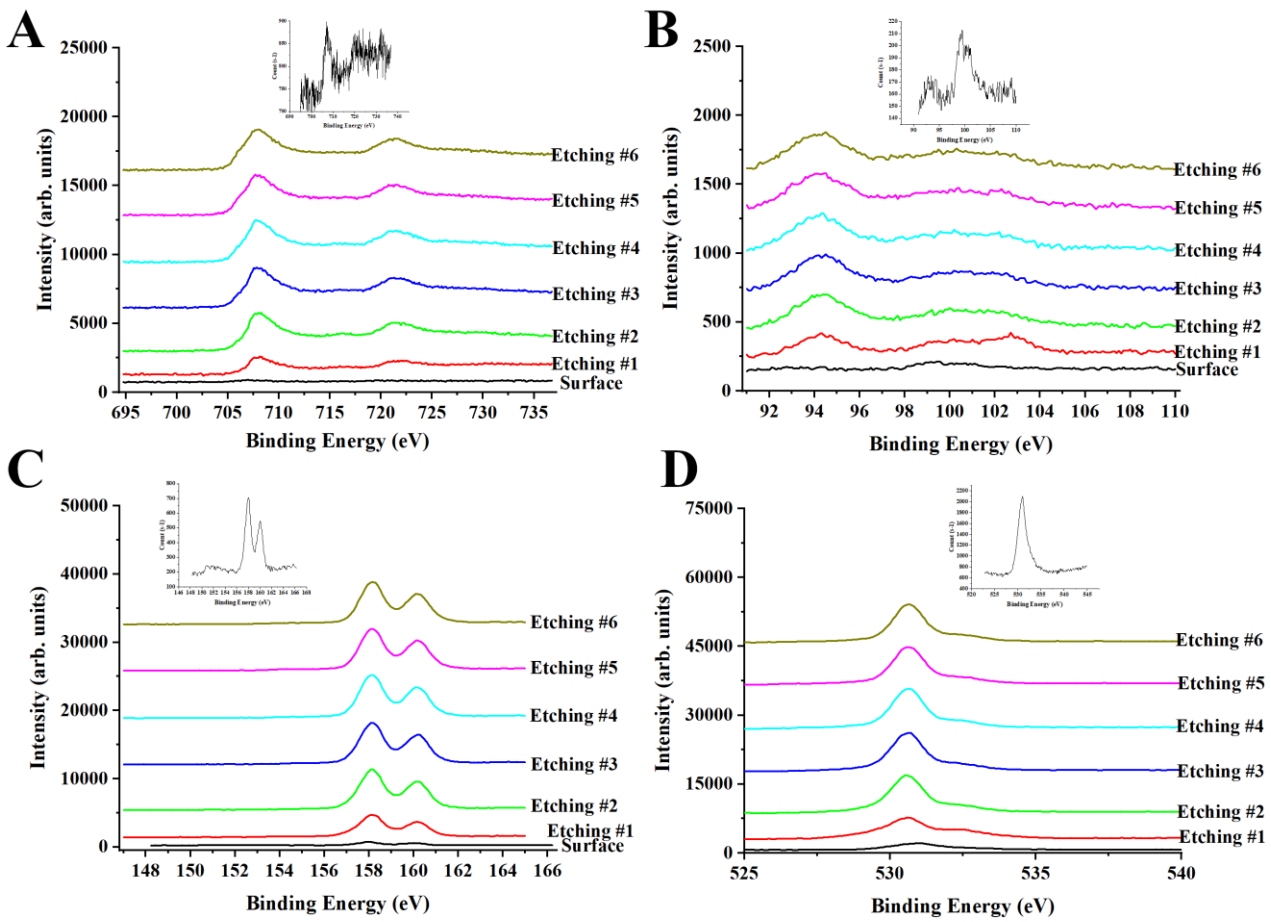

Fig 4. *Si:YIG XPS spectra acquired from the surface and after each of 6 consecutive etchings with Ar ions for Fe 2p (A), Si 2p (B), Y 3d (C), and O 1s (D) spectral regions. The insets in Figure A-D show a magnified XPS spectrum acquired from the sample surface.*

b. Magnetic characterization

For the magnetic resonance studies the sample was positioned on top of a short-circuited coplanar microstrip transmission line fabricated from 0.01 inch thick Rogers RT/Duroid® 5880 laminated substrate (Fig. 5). A DC bias magnetic field H_0 was applied parallel to the sample plane and directed along the transmission line. The reflection coefficient S_{11} which is the ratio of the microwave power reflected from the measurement cell to the incident microwave power (expressed in decibels) was then measured with a 3-8 GHz scalar network analyzer under various experimental conditions as described below The dips in S_{11} vs. f reflection characteristics indicate the microwave power absorption in the ferrite sample due to the ferromagnetic resonance. In that way the magnetic resonances frequencies were experimentally determined.

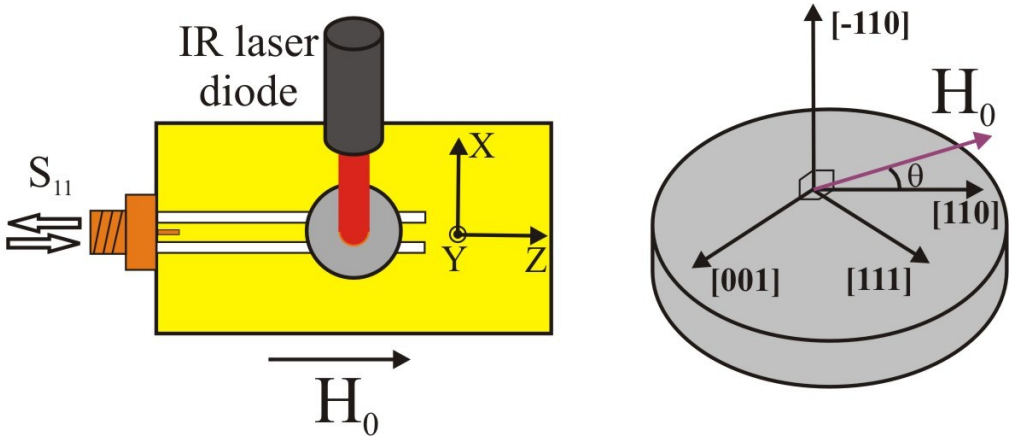

Fig.5 *(Left) Schematics of experimental set-up for the investigation of optical irradiation influence on the magnetic resonance frequency. (Right) Relative in-plane orientation of the cardinal crystallographic axes (note that [110] and [-110] axes in cubic crystal are physically equivalent).*

The FMR resonance frequency vs. bias magnetic field orientation dependence for the H_0 in the (110) crystallographic plane is described by the following equation [18, 26]:

$$f(H_0,\theta)=\gamma\sqrt{H_0+4\pi M(N_y-N_z)+2(1-2\cos^2(\theta_M)-\frac{3}{8}\sin^2(2\theta_M))H_k}\times \sqrt{H_0+4\pi M(N_x-N_z)+(2-\cos^2(\theta_M)-3\sin^2(2\theta_M))H_k}. \quad (18a)$$

Here $4\pi M$ is the saturation magnetization, $H_k = K_1/M$ is the cubic anisotropy field value, and N_i (i=x, y, z) are the demagnetization factors along the sample principal axes. We assume that Z axis coincides with bias magnetic field direction, Y is along the disk normal and X is in-plane, orthogonal to Z and Y (see Fig. 5). Furthermore, θ is the angle of bias magnetic field orientation (as shown on Fig. 3) and θ_M is the angle between the direction of the static magnetization vector M and [110] axis in the crystal plane. In general, they are not the same and θ_M is a function of θ, H_0 and material magnetic parameters such as H_k. But, taking into account that usually $H_k << H_0$, one may assume that magnetization direction coincides with the bias magnetic field direction and, therefore, angle θ_M may be the same value as the angle θ shown in Fig 3 and also in Fig.4b.

For a sample of cylindrical shape, due to the symmetry considerations we can introduce $N_{\|}$ - the demagnetization factor along the cylinder axis and $N_{\perp}$ - is the demagnetization factor along arbitrary in-plane direction. In the case of Eq. (18a) and given coordinate system this corresponds to $N_x = N_z = N_{\perp}$ and $N_y = N_{\|}$. Then the angular dependence is given by

$$f(H_0,\theta) = \gamma\sqrt{H_0 + 4\pi M_{eff} + 2(1-2\cos^2(\theta_M) - \frac{3}{8}\sin^2(2\theta_M))H_k} \times \sqrt{H_0 + (2-\cos^2(\theta_M) - 3\sin^2(2\theta_M))H_k}, \quad (18b)$$

where $4\pi M_{eff} = 4\pi M(N_{\|} - N_{\perp})$. For our specific sample shape and dimensions (see above) we calculated demagnetization factors to be $N_{\perp}$=0.107and $N_{\|}$=0.786.

Finally, for the bias field oriented along the easy [001] axis, one should substitute $\theta_M=\pi/2$ in Eq.(18b) to get

$$f(H_0,\theta) = \gamma\sqrt{(H_0 + 2H_k + 4\pi M_{eff})(H_0 + 2H_k)} \quad (19).$$

It is seen that for bias along this highly-symmetrical axis the effect of cubic anisotropy reduced to substitution $H_0 \to H_0 + 2H_k$ in expression for isotropic ferrite [18].

The measured f vs. H_0 plot for the dominant (lowest-frequency) magnetic mode for the H_0 directed along [001] axis is shown in Fig.6a. It demonstrates a quasi-linear trend for larger bias magnetic field values which is typical for the in-plane magnetized ferrite sample with low cubic anisotropy field [18]. The red line shown in the Figure is the theoretical fit using eq. (19).

The effective gyromagnetic value γ determined from a fit of experimental data was found to be equal to 2.82±0.02 MHz/Oe, saturation magnetization $4\pi M$=947±96 G, and H_k=271±13 Oe. The reduced value of saturation magnetization (in comparison with pure (unsubstituted) YIG [27]) is expected since in pure YIG magnetization arises as a difference between Fe^{3+} magnetic moments in tetrahedral sites and octahedral sites: $M=M_{tetr}-M_{oct}$ and non-magnetic Si^{4+} are known to preferentially enter tetrahedral sites [14] thus reducing both M_{tetr} and net magnetization. The positive value of H_k (in contrast to the negative value in pure YIG) is consistent with the previously reported data on Si:YIG of similar composition [2, 28]. On the

contrary to nearly isotropic Fe^{3+}, the Fe^{2+} ions substituted in the YIG give a large positive contribution to the first-order cubic anisotropy constant K_1 (see Ref. [11]). Thus, if the amount of ferrous ions is large enough, they may compensate for negative K_1 of pure YIG and lead to a positive cubic anisotropy field.

We verified the obtained value of saturation magnetization by applying a molecular field theory, detailed in [28]. According to it, at T = 0 K the magnetization per mole is given by

$$M(0) = M_{tetr}(0) - M_{oct}(0)$$

where, for the garnet with chemical composition $Y_3Fe_{5-x}Si_xO_{12}$, the sublattice magnetizations can be expressed as

$$M_{oct}(0) = g\mu_B N_A \left(\frac{5}{2}(2-x) + 2x \right), \quad M_{tetr}(0) = g\mu_B N_A \frac{5}{2}(3-x)$$

Here g=2 is the Landé factor, μ_B the Bohr magneton, N_A – the Avogadro's number, and we took into account that 1) Si ions go to tetrahedral lattice and 2) Fe^{2+} ions which appear in octaherdal lattice posess reduced magnetic moment in comarsion to Fe^{3+}. The temperature dependence of sublattice magnetizations is governed by the Brillouin functions of angular momentum 5/2 [28]:

$$M(T) = M_{tetr}(T) - M_{oct}(T)$$

$$M_{tetr}(T) = M_{tetr}(0) B_{\frac{5}{2}} \left(g\mu_B \frac{5}{2} \frac{\left[N_{tetr} M_{tetr}(T) + N_{oct-tetr} M_{oct}(T) \right]}{kT} \right)$$

$$M_{oct}(T) = M_{oct}(0) B_{\frac{5}{2}} \left(g\mu_B \frac{5}{2} \frac{\left[N_{oct} M_{oct}(T) + N_{oct-tetr} M_{tetr}(T) \right]}{kT} \right)$$

where N_{oct}, N_{tetr}, $N_{oct\text{-}tetr}$, are the intra- and inter- lattice coefficients of the molecular field. By substituting the values of molecular field coefficients taken from [28], we obtained for x=0.51 from theoretical calculations M(0 K) = 1469 G, and M (300 K)=929 G, the latter is in close agreement with the experimental data.

Further, we have measured the angular dependence of the profiles for a fixed magnitude of H_0. The sample was rotated around the cylinder axis in such a way that the bias field always

remained in-plane and corresponding changes in magnetic resonance frequency were recorded (Fig. 6b). The data show strong angular dependence of f_r caused by the internal cubic anisotropy of the sample.

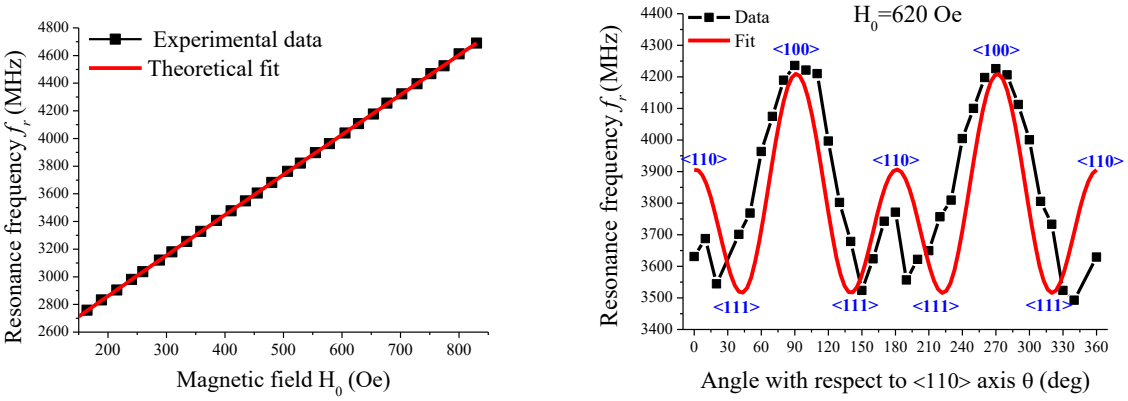

Fig.6 *(Left) Experimental f_r vs. H_0 dependence for the disk Si:YIG sample at room temperature together with theoretical fit. (Right) Magnetic resonance frequency angular dependence on bias field in-plane direction together with theoretical fit and presumable directions of crystallographic axes.*

The data presented in Fig.6b was fitted using theoretical expression (18b) and previously obtained value of γ. The theoretical graph (solid curve in Fig. 6b) demonstrates acceptable agreement with the experimental data. However, here the fit magnetic parameters differ from those used for Fig. 6a, namely, smaller value of H_k=55±10 Oe was obtained. It has to be assumed that the mode observed in this experiment was not a uniform FMR but rather one of the spatially non-uniform magnetostatic modes of cylindrical ferrite resonator [18]. Those modes have dispersion equations that are different from (18b), besides, their frequencies are strongly affected by the presence of metal screens near to resonator (in our case - the top copper surface of coplanar line). Nevertheless, the data in Fig.6b definitely proves the anisotropic properties of our sample and thus its single-crystal nature. Assuming that the orientation dependence for the magnetostatic mode is *qualitatively* the same as for FMR, we have used these results to identify the in-plane positions of all three principal cubic crystal axes, namely [001], [110], and [111] (as

shown in Fig. 6b). We can see that [001] is the easy axis, [111] is hard and [110] is intermediate, in accordance to the positive value of the cubic anisotropy field H_k. Further measurements, described in the following section, were undertaken with a bias field oriented along the easy [001] axis.

4. Results and Discussion

For the photomagnetic measurements, the disk was illuminated by a focused beam from an infrared laser diode (ADL-80X01TZ, Arima Lasers Corporation) with λ=808 nm (see Fig. 5). The direction of the light beam was normal to the sample's surface. The incident optical power P_{opt} was controlled by tuning the current flowing through the laser diode and varied from 0 to 75 mW. The investigation of laser output revealed that it consists of a mix of linearly polarized (≈90 % of total power) and non-polarized (≈10 % of total power) components (Fig.S2-Supplement). One of the goals of this work was to demonstrate the existence of polarization-dependent photomagnetic effect. And, as evident from this work, even a modest amount of linear polarization of the incident laser is sufficient to demonstrate it. The incident optical power was completely absorbed and either converted to heat or spent on the excitation of the conductivity electrons which further hop from one octahedral crystallographic position to others.

From the data presented in Ref.[29] we can estimate the optical absorption coefficient α being approximately 80±10 cm^{-1} for λ=800 nm for the pure YIG. Assuming this value for Si:YIG and making use of the Beer-Lambert law: $I(h) = I_0 \cdot \exp(-\alpha \cdot h)$, we can estimate that the incoming light is almost fully absorbed at sample's thickness of $h \approx 3/\alpha$ which is equal to ≈0.375 mm. Further taking into account that any light that passes through the sample is then reflected back from metal surface of coplanar line and travel through the sample again, we can safely assume that for the given sample thickness h=0.27 mm, all the optical radiation was absorbed by ferrite.

First, the measurements were conducted at room temperature. The experimentally recorded reflection characteristics for the Si:YIG sample measured for different laser illumination power

are presented on Fig. 7a. One can see a clear downshift of resonance frequency which is linearly proportional to the applied optical power, see Fig. 7b. It now remains to determine, which part of this effect is caused by photo-stimulated electrons hopping and which originates from the sample's heating. In order to evaluated this, we prepared the reference sample having the same geometrical dimensions but made from pure (undoped) polycrystalline YIG ($Y_3Fe_5O_{12}$). Since pure YIG does not have measurable amounts of impurity atoms, it is not expected to show a photomagnetic response. Moreover, polycrystalline structure of the sample will "average out" any crystallography-conditioned effects given the direct measure of heating influence. The measurements on the reference sample were conducted under the same experimental set-up as for the Si:YIG. Only the bias magnetic field H_0 was adjusted in such way to get the same initial frequencies as in the investigated sample.

The results for the reference sample are shown in Fig 7b by red dots. Comparison between the two sets shows that Si:YIG does demonstrate larger frequency shifts, which may be explained either by the effect of photoinduced variation of magnetic anisotropy or by some difference in physical properties of samples (like optical absorption or specific heat capacity).

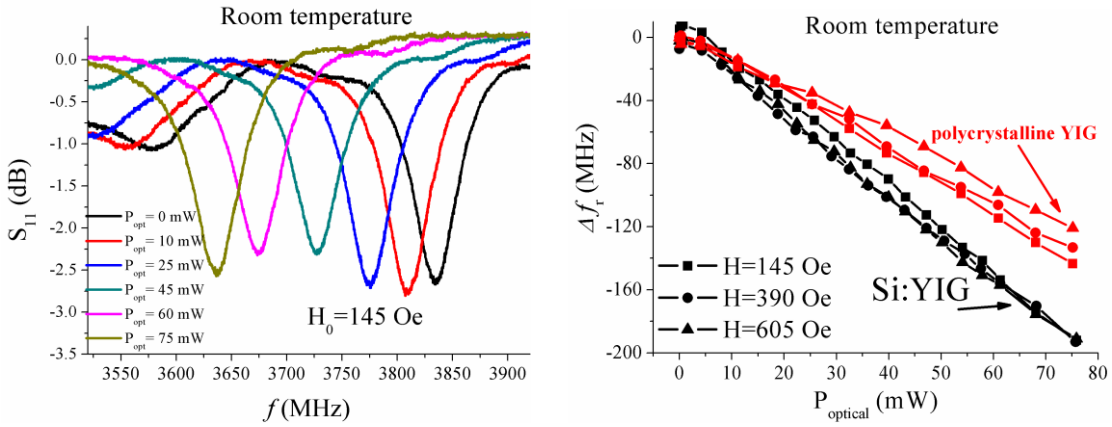

Fig.7. *(Left) Reflection characteristics of Si:YIG sample measured for fixed value of bias magnetic field and different values of laser diode output power at room temperature; (Right) Comparison between experimentally measured optically induced FMR frequency shifts in Si:YIG sample (black dots) and polycrystalline YIG sample (red dots) with the same geometrical dimensions at room temperature.*

Nevertheless, the difference between both cases is relatively small, suggesting that at room temperature thermal heating is responsible for the large part of the net measured frequency change and photomagnetic phenomena account for just a fraction of it.

Better isolation of the photomagnetic effect was expected in the case of low-temperature measurements. During the cryogenic experiments the microstrip line with sample was placed inside a thermo-isolated casing and completely immersed in liquid nitrogen (T=77 K). Since nitrogen was in direct contact with the ferrite sample, it efficiently absorbed all the excessive heat caused by irradiation, stabilizing its temperature at the abovementioned mark. The experiments conducted in liquid nitrogen indeed showed that whereas Si:YIG continued to demonstrate optically induced magnetic resonance frequency shift, for the reference sample the observed frequency variation was negligible even at maximum applied optical power, reaching 7 MHz at most (Fig.S3-supplement) which is on the verge of experimental error. Hence the immersion of the sample in liquid nitrogen removes the possibility that the observed effect might arise from the radiation-induced heating of the sample.

First, the sample was oriented in such a way that H_0 || [001] and a resonance frequency vs. field dependency was recorded, see Fig. 8. The resonance frequencies became noticeably larger due to the increase in both saturation magnetization $4\pi M$ and cubic anisotropy field H_k at cryogenic temperatures [2], see expression (19). For the theoretical calculations we used M (77 K) = 1423 G, evaluated using molecular field theory [28], and received γ=2.69±0.01 MHz/Oe and H_k=748±6 Oe.

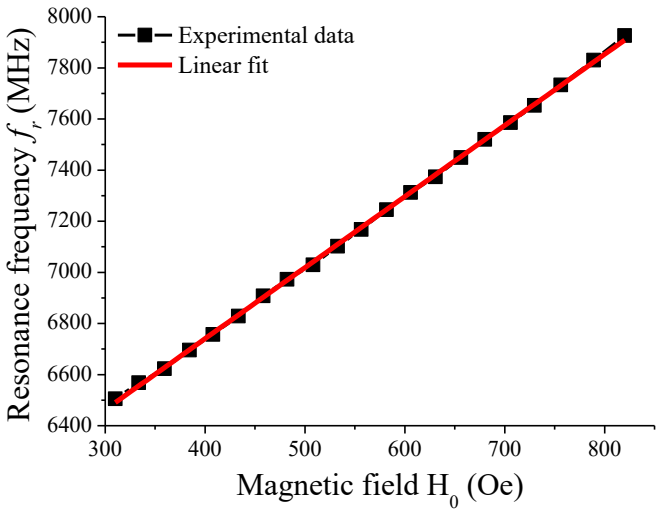

Fig.8. *Experimental f_r vs. H_0 dependence for the disk Si:YIG sample at liquid nitrogen temperature with theoretical fit.*

Next, the magnetic field value was fixed and we investigated the dependence of resonance frequency on the incoming light polarization vector $\vec{P}$ orientation with respect to the sample's crystallographic axes. The reorientation of the polarization vector was realized by mechanical rotation of the infrared laser diode. Since the light beam was normal to the ferrite surface, the vector $\vec{P}$ direction remained in the sample's plane (which coincides with the crystallographic (110) plane), and only the angle between $\vec{P}$ and cardinal axes was alternating during the experiment. The orientation angle φ was measured from the in-plane [001] axis direction with an accuracy of ±5°.

Figure 9a shows a change in the sample reflection characteristic induced by the linearly polarized light with the same optical power but different orientation with respect to the [001] crystallographic axis. A strong dependence of photoinduced frequency shift on polarization vector orientation was observed. Fig. 9b shows the frequency shift measured at the same H_0 and P_{opt} for different values of angle φ. When $\vec{P}$ makes a full turn, a frequency shift demonstrates a periodical variation with two local maxima and two minima per full circle. Such behavior is consistent with the theoretical model presented in the following section. Moreover, this data

definitely proves the photomagnetic nature of the investigated effect. Indeed, for thermal effect one may expect the sample heating to be independent of polarization orientation and the frequency shift should remain approximately the same for arbitrary φ angle. Even if we consider

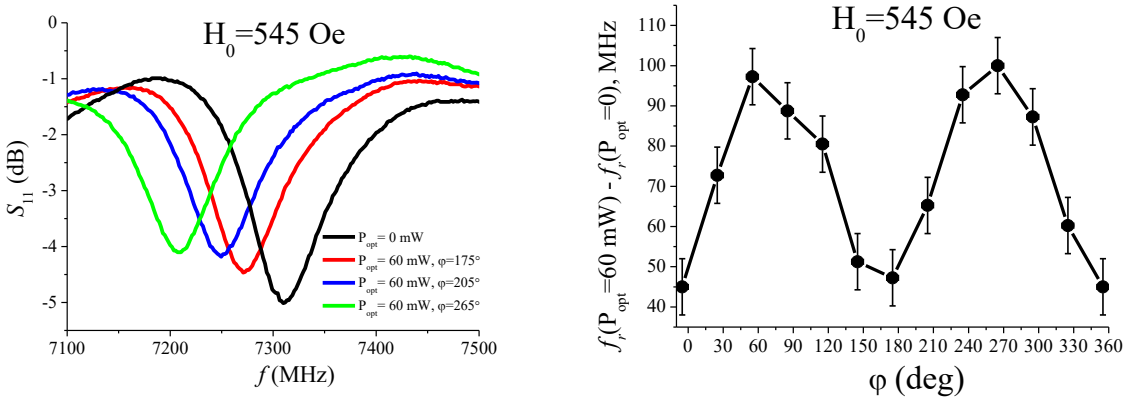

***Fig.9**. Photoinduced resonance frequency shift for the Si:YIG sample at liquid nitrogen temperature for different in-plane orientations of the polarization vector: (Left) Reflection characteristics, (Right) frequency shift variation with angle φ between $\vec{P}$ and [001] axis.*

such an effect as photo-induced linear dichroism, reported for Si:YIG at 1.5 K in Ref.[7], the magnitude of this effect (< 2%) is too small to account for the observed frequency shift variations.

Based on the data shown in Fig. 9b, it can be concluded that the maximum photoinduced frequency shift takes place when $\vec{P}$ is oriented orthogonally to <001> axes and thus is aligned with <110> axes (see Fig.5), namely φ≈90° and φ≈270°. On the contrary, for φ≈0° and φ≈180°, when $\vec{P}$ coincides with <001> axes, the frequency shift is minimal. During the next set of measurements, the polarization orientation was fixed at optimum direction of φ=270° and optically induced magnetic resonance frequency shift was investigated as a function of the applied optical power. Fig. 10a shows the measured reflection coefficient for different values of P_{opt}. The resonance curve steadily shifts downward at the same time retaining is profile and resonance linewidth. The observed variations in resonance absorption value may be ascribed to the frequency dependence of the transmission line background signal. Hence, the frequency tuning is not

accompanied by an increase in intrinsic losses and the primary photoinduced effect consists of the variation of some internal magnetic parameter, which, in turn, results in frequency change. Similar profiles were recorded at two other values of bias magnetic field H_0 (Fig.S4-Supplement).

The frequency shift vs. applied optical power dependences are presented in Fig. 10b. The measurements at three different values of applied field produced nearly identical results. The overall Δf_r vs. P_{opt} trend is generally linear, although some nonlinear deviations are seen at low optical power values. The maximum obtained frequency shift was –130 MHz for P_{opt} =75 mW with average frequency tuning efficiency of (1.73±0.06) MHz/mW.

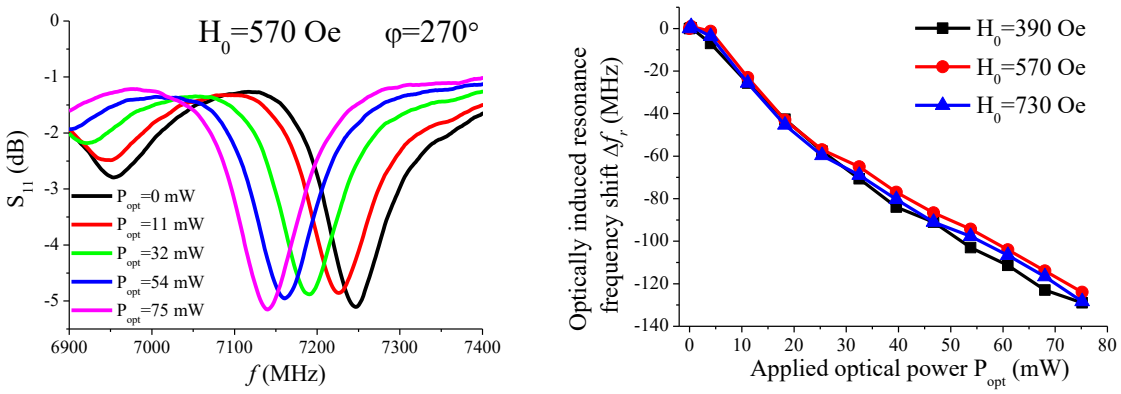

Fig.10. *Photoinduced resonance frequency shift for the Si:YIG sample at liquid nitrogen temperature: (Left) reflection characteristics modification with optical power, (Right) frequency shift dependence on applied optical power. All data taken for fixed orientations of the infrared radiation polarization vector.*

To exclude from consideration the other magnetic and electrophysical parameters of ferrite under investigation, we compared in Fig. 11a the normalized values of experimentally measured optically induced frequency shift with normalized theoretical calculations of $(4n_{[111]}-1)$ term (See Fig. 1). One can see that the curves demonstrate qualitatively similar character. One fundamental discrepancy is in the fact that experimentally measured frequency shift does not reach zero at φ=0° and 180° contrary to theoretical data. This may be caused by the following phenomena. Firstly, laser diode radiation, besides linearly polarized light, contains

some portion of nonpolarized light (as discussed before) and nonpolarized light intensity affects the ferrite sample in the identical way regardless of the laser source orientation. Since photoinduced anisotropy is much more sensitive to low power optical signal levels (see discussion under Fig. 2), even a small intensity non-polarized light can induce a rather large uniaxial anisotropy and correspondent angle-independent ground-level frequency shift. In order to verify that, another experimental curve was plotted on Fig. 11b with ground-level frequency shift being mathematically subtracted according to $\frac{\Delta f_r^*}{\Delta f_{r\max}^*}(\varphi) = \frac{f_r(\varphi) - f_r(\varphi = 0)}{f_r(\varphi = 3\pi/2) - f_r(\varphi = 0)}$. One can see that this time the coincidence has improved.

Another cause can be attributed to the assumptions made during the derivation of Eq. (11) regarding determination the direction of anisotropy axis. It is possible, that for angles close to φ=0°, 180° some of the assumptions made there become incorrect and cause additional errors to the final formula.

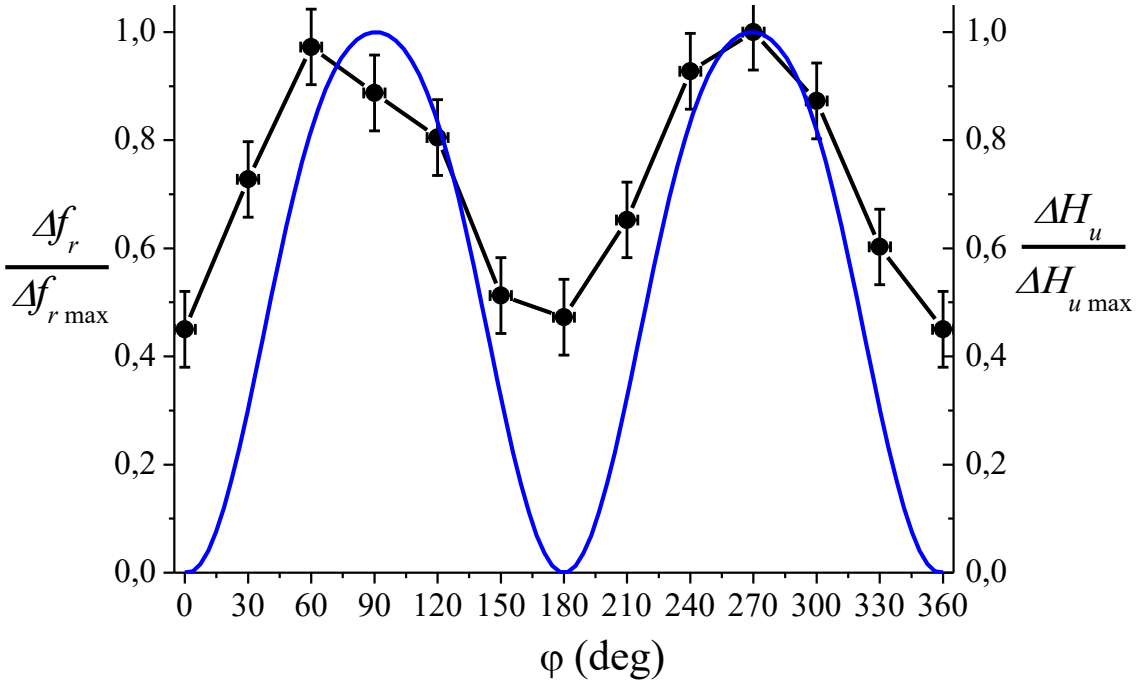

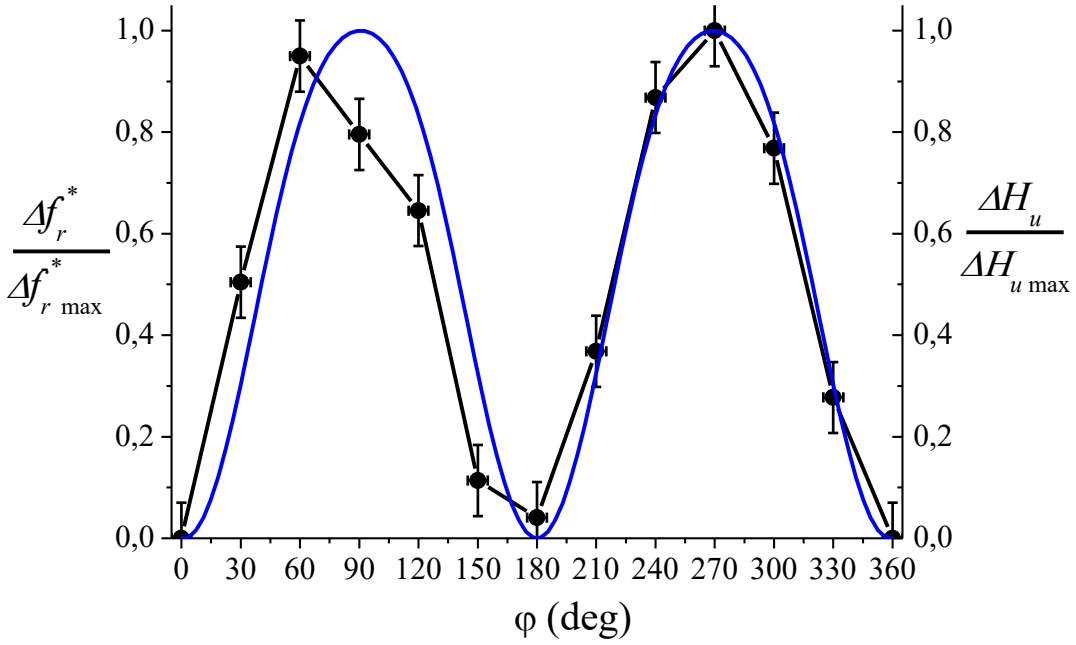

Fig. 11. *(Top) Comparison between experimentally measured normalized photoinduced frequency shift and theoretical calculations based on optically stimulated uniaxial anisotropy model. (Bottom) Same dependence but with ground level frequency shift subtraction.*

Finally, Fig. 12 demonstrates the measured FMR frequency shift, normalized to the maximum registered value and plotted against optical intensity, together with theoretical calculations of $(4n_{[111]}-1)(I)$, see Fig 2. As follows from Eqs. (13) and (16), Δf_r and $(4n_{[111]}-1)$ should be proportional to each other, thus plotting normalized values on a single graph allows us to verify this assumption directly. A decent correspondence is clearly seen, justifying the proposed theoretical model presented in Section 2.

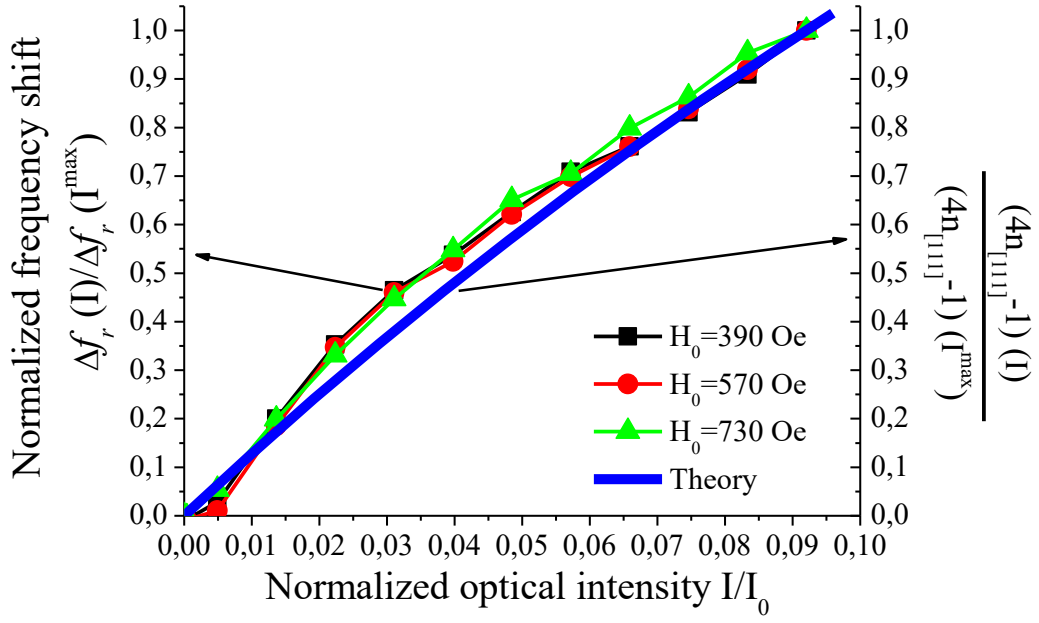

Fig.12. *Normalized photoinduced resonance frequency shift versus applied optical intensity together with the theoretical line for normalized* $(4n_{[111]}-1)$ *value (see text for details) for optimal orientation of the infrared radiation polarization vector.*

Finally, we address the difference between thermal heating effect and magnetooptical effect which is a key question in this research. In order to distinguish among those two effects we made a comparison between Si:YIG and Si-free polycrystalline YIG reference sample (of nearly the same dimensions). Due to identical crystal structure and nearly similar chemical composition these materials should have similar optical absorption properties, specific heat, thermal conductivity etc. However, since polycrystalline YIG sample lacks Si doping and has extremely low electric conductivity, it is not expected to have any magnetooptical effect.

Therefore, it is reasonable to infer from data at 77 K and room temperature that any measurable difference in behavior between Si:YIG and polycrystalline YIG sample should be attributed to magnetooptical effect. As shown on the right panel of Fig. 5, at room temperature both samples have a comparable frequency shift. Since for polycrystalline sample it is definitely due to the heating, we assume that in the case of Si:YIG frequency shift from heating have approximately the same value. Thus, at RT the optical excitation of electrons is responsible only

for small portion of the observed frequency shift effect (which is exactly what was stated in the conclusions).

On the other hand, during the 77 K measurements the liquid nitrogen environment acts as a heat sink, quickly removing the excess heat from the sample and keeping it temperature nearly constant. As shown on Fig. S3 of Supplement, under this condition polycrystalline YIG shows only negligible frequency shift, which proves that its temperature remains nearly unchanged. On the contrary, under the same condition Si:YIG showed more than 120 MHz frequency shift. Again, comparing it with reference sample we conclude that in this case almost all frequency shift should be attributed to magnetooptical effect, and not to any thermal effects.

Taking into account sample dimension, YIG density (5.17 g/cc), and specific heat (C=590 J/kg/K), we estimated that it requires only 4 mJ to heat our sample by 1 K. Thus the 75 mW laser will heat thermally insulated sample by 19 C. One anticipates somewhat rapid transfer of thermal energy from the sample to surrounding liquid nitrogen at 77 K and the sample temperature to remain the same. At room temperature, however, any transfer of thermal energy from the sample to surrounding air is likely to be a slow process leading to some heating. The equilibrium temperature of the sample at RT may be estimated from the FMR frequency shift of – 120 MHz. If attributed to thermal heating and the resulting decrease in the magnetization $4\pi M$, then it requires the magnetization changes of $\Delta(4\pi M) \approx$ -120 MHz/(2.8 MHz/G) ≈ -43 G. For pure YIG at RT the magnetization changes at the rate -4 G/K, sample heating by +11 K above the room temperature will account for the shift in FMR frequency. The estimated heating of the sample by 11 C seems to be quite reasonable value."

5. Conclusions

It was experimentally and theoretically demonstrated that in Si:YIG the electron population density distribution among Fe^{2+} ions in crystallographically equivalent octahedral sites at liquid nitrogen temperature can be modified in a controlled manner by irradiation with a linearly polarized infrared beam. The changes in occupation numbers manifest themselves (among others) as an appearance of an additional uniaxial anisotropy field. Under some assumptions, it was

derived that for the considered experimental configuration the photoinduced anisotropy axis direction may be assumed fixed and its magnitude depends on the difference between the population density at the specific site and its equilibrium value $\Delta n_{[111]} = \left(n_{[111]} - \frac{1}{4} \right)$. Theoretical formulae that elucidate the effect of photoinduced anisotropy on experimentally registered FMR frequency were obtained. The developed model predicts a strong dependence of anisotropy's magnitude on incident light's polarization vector orientation with respect to crystallographic axes, which was experimentally confirmed from FMR frequency shift measurements. After the orientation-independent frequency shift subtraction, the coincidence between theory and experiment became satisfactory. The dependence of FMR frequency shift on light intensity was predicted to be nonlinear with saturation at large intensity levels. Experimentally, however, only a linear Δf_r vs. P trend was confirmed, as appropriate to the initial part of the dependence. That happened since the laser source used in experiments provides output intensity much lower than that required for the nonlinearity to reveal itself.

The studied Si-substituted YIG can be applied in the development of optically controlled ferrite signal processing devices, which are based on the FMR effect and operate at a centimeters wavelength frequency band. In these devices, the operating frequency and other related characteristics, in addition to traditional H field tuning, can be altered by optical irradiation in an energy-efficient and contactless manner. Since laser diode source can be rather tiny and lightweight (in comparison to a magnetic field tuning system), this approach will potentially produce said devices miniaturization. The optical tuning effect reported here was manifested in full only at liquid nitrogen temperature. The similar phenomenon observed at room temperature was attributed mostly to the sample's heating by incident light. The influence of electron density redistribution effect on FMR frequency shift at room temperature is currently unknown and yet to be determined. Therefore, the perspective of practical utilization of optically controlled magnetic anisotropy for signal processing devices tuning at ambient conditions remains to be investigated.

Supplementary Material

The supplementary material contains the following figures.

Fig. S1 XRD spectrum of monocrystalline $Y_3Fe_{4.49}Si_{0.51}O_{12}$sample acquired using K_α line of Fe ($\lambda = 1.93735$ Å). **Fig. S2** Laser diode output power dependence on the orientation angle of the rotating polarizer. **Fig. S3** Optically induced FMR frequency shift in polycrystalline YIG disk sample immersed in liquid nitrogen. **Fig. S4.** The measured reflection coefficient for different values of P_{opt} (similar to those shown in Fig. 8a of the manuscript) at two other values of bias magnetic field,H_0=390 Oe and H_0=730 Oe. **Fig. S5.** The polar angles δ_2, δ_3 between vectors $\vec{V}_2, \vec{V}_3$ and [001] dependence on the incident light polarization orientation angle (theoretical calculations).

Data Availability

Data contained in this manuscript are available from the corresponding author upon request.

Acknowledgements

This study was partially supported by the MITACS Accelerate grant (IT31144) and the Natural Sciences and Engineering Research Council of Canada (NSERC) Discovery Grant (RGPIN-2024-04811). YS was supported by the MITACS Elevate grant (IT25574) and the MITACS Accelerate grant (IT31144). The authors would like to thank Dr. V. F. Kovalenko for providing the Si:YIG samples for investigation. The authors would like to thank Dr. Guosheng Wu for his assistance with XPS measurements. The authors would like to thank Michael Sorokopud for his assistance with the XRD spectrometer. The research at Oakland University was supported by grants from the National Science Foundation (ECCS-2415328, ECCS-EAGER-2236879) and the Air Force Research Laboratory, Dayton, Ohio. The research at AFRL was supported by a grant from the AFOSR (Award No. FA9550-23RXCOR001).

References

[1] V. F. Kovalenko, and E. L. Nagaev, “Photoinduced magnetism”, Sov. Phys. Usp., vol.29, pp. 297–321, 1986.

[2] R. W. Teale, D. W. Temple, and D. I. Weatherley, “Magnetic anisotropy and magnetic anneal in silicon-doped yttrium iron garnet”, Phys. C : Solid State Phys., vol. 3, pp. 1376-1387, 1970.

[3] I. I. Davidenko, S. N. Lyakhimets, and V. F. Kovalenko, “Phenomenological description of spin-reorientational transitions in YIG:Si induced by linearly polarized light”, Phase Transitions: A Multinational Journal, vol. 50, no. 4, pp. 255-263, 1994.

[4] V. F. Kovalenko, E. S. Kolezhuk, and P. S. Kuts, “Effect of linearly polarized light on domain structure in a Y3Fe5-xSixO12 plate”, Sov. Phys. JETP, vol. 54, no. 4, pp. 742-745, 1981.

[5] R. W. Teale, and D. W. Temple, “Photomagnetic anneal a new magnetooptic effect in Si-doped yttrium iron garnet”, Phys. Rev. Let., vol. 19, no. 16, pp. 904-905, 1967.

[6] P. S. Kuts, V. F. Kovalenko, and V. A. Ruban, “Influence of thermomagnetic treatment and light exposure on the magnetic properties of $Y_3Fe_{5-x}Si_xO_{12}$ crystals”, Soviet Physics Journal, vol. 19, pp. 1222-1225, 1976.

[7] J. F. Dillon, Jr., E. M. Gyorgy, and J. P. Remeika, “Photoinduced magnetic anisotropy and optical dichroism in silicon-doped yttrium iron garnet”, Physical Review Letters, vol. 22, no. 13, pp. 643-645, 1969.

[8] A. V. Zhukovskiy, V. F. Kovalenko, P. S. Kuts, B. P. Nam, A. S. Khe, “Light influence on magnetic anisotropy of $Y_3Fe_5O_{12}$:Si epitaxial films”, Solid State Physics, vol. 27, no. 9, pp. 2841-2843, 1985.

[9] K. Uematsu, M. Deguchi, and Y. Kito, Photoinduced change in SWR spectra of Si-deposited YIG thin films”, J. Magn. Magnet. Mater., vol. 35, no. 1-3, pp. 65-67, 1983.

[10] S. Krupička, Physik der ferrite und der verwandten magnetischen oxide, Vieweg+Teubner Verlag, Wiesbaden, 1973, 780 p.

[11] P. Hansen, “Magnetic Anisotropy and Magnetostriction in Garnets” in: Physics of Magnetic Garnets, ed. by A. Paoletti (North Holland, Amsterdam, 1978), p. 56–133.

[12] D.G. Makarov, O.V. Tychko, V.F. Kovalenko, “Photoinduced changes of magnetic anisotropy in substituted iron garnet”, Journal of Alloys and Compounds, vol. 369, no. 1-2, pp. 222–226, 2004.

[13] R.W. Teale, D.I. Weatherley, B.T. Sharp, “Photosensitivity of the magnetic anisotropy in silicon-doped yttrium iron garnet”, Physics Letters A, vol. 30, no. 3, pp.155-156, 1969.

[14] T. Merceron, “Electronic Hopping Process in Silicium or Calcium Doped Yttrium-Iron Garnets”, Phys. Stat. Sol. (a), vol. 15, pp. 539-544, 1973.

[15] T. S. Hartwick and J. Smit, ”Ferromagnetic Resonance in Si-Doped YIG”, Journal of Applied Physics, vol. 40, No 10, pp. 3995-4001, 1969.

[16] I. R. Shafarevich, A. O. Remizov, Linear Algebra and Geometry. - Springer-Verlag, Berlin, Heidelberg, 2013. - 526 p.

[17] V.F. Kovalenko, S. N. Lyakhimets, “Temperature dependence of a photoinduced spin-orientation effect in $Y_3Fe_5O_{12}$:Si”, Sov. Phys. Solid State, vol. 26, no. 10, pp. 1817–1820, 1984.

[18] A. G. Gurevich and G. A. Melkov, Magnetization Oscillations and Waves. -New York: CRC, 1996.

[19] Pena-Garcia R., Guerra Y., Santos FEP., Almeida LC., Padron-Hernandez E. “Structural and magnetic properties of Ni-doped yttrium iron garnet nanopowders”, J. Magn. Magn. Mater. 2019; 492(15):165650.

[20] Shi L., Wang X., Gao K., Chen H., Yan W. “Growth of homogeneous-phase YIG grains on Si substrates and their optical properties on a micron scale”, Ceram. Int. 2021; 47:14067-14074.

[21] Li M., Jin L., Zhong Z., Tang X., Yang Q., Zhang L., Zhang H. “Impact of interfacial chemical state on spin pumping and inverse spin Hall effect in YIG/Pt hybrids”, Phys. Rev. B. 2020; 102: 174435.

[22] James R. W., The optical principles of the diffraction of X-rays. – London G. Bell & Sons Ltd., 1954 – 624 p.

[23] Torres C., Alejos O., Hernandez-Gomez P., Munoz M., Francisco C. “Magnetic aftereffects in Si-Doped YIG”, IEEE Trans Magn. 2002; 38(5):3024-3026.

[24] Caland J.P., Medrano C.P.C., Caytuero A., Baggio-Saitovitch E., Litterst F.J., Soares J.M., Cabrera-Baez M., Padron-Hernandez E., Marques T., Guerra Y., Viana B.C., Santos F.E.P., Pena-Garcia R. “Preferential site occupancy of Ni ions and oxidation state of Fe ions in the YIG crystal structure obtained by sol-gel method”, J. Alloys Compd. 2020; 849:156657.

[25] Musa M.A., Azis R.S., Osman N.H., Hassan J., Zangina T. “Structural and magnetic properties of yttrium iron garnet (YIG) and yttrium aluminum iron garnet (YAIG) nanoferrite via sol-gel synthesis”, Res. Phys. 2017; 7:1135-1142.

[26] L. R. Bickford, Jr, “Ferromagnetic resonance absorption in magnetite single crystals”, Physical Review, vol. 78, no. 4, pp. 449-457, 1950.

[27] Landolt–Börnstein Numerical Data and Functional Relationships in Science and Technology Series, Group III Crystal and Solid State Physics. Vol. 4a / D. L. Huber; ed. K.–H. Hellwege, A. M. Hellwege. – New York : Springer–Verlag, 1970. – 367 p.

[28] Hansen, P., Röschmann, P. & Tolksdorf, W. Saturation magnetization of gallium-substituted yttrium iron garnet. J. Appl. Phys. 45, 2728–2732 (1974).

[29] J.F. Dillon, “Optical absorptions and rotations in the ferrimagnetic garnets”, J. Phys. Radium, vol. 20, no. 2-3, pp.374-377, 1959.